Magnetic Field Reversal around an Active Fast Radio Burst

Di Li (dili@nao.cas.cn)
National Astronomical Observatories, Chinese Academy of Sciences;University of Chinese Academy of Sciences, Beijing 100049, China https://orcid.org/0000-0003-3010-7661

Shi Dai
Western Sydney University

Yi Feng
National Astronomical Observatories, Chinese Academy of Sciences, Beijing 100101, China

Yuan-Pei Yang
Yunnan University https://orcid.org/0000-0001-6374-8313

Yongkun Zhang
National Astronomical Observatories, Chinese Academy of Sciences, Beijing 100101, China

C.H. Niu
National Astronomical Observatories, Chinese Academy of Sciences

P. Wang
National Astronomical Observatories, Chinese Academy of Sciences

Mengyao Xue
National Astronomical Observatories, Chinese Academy of Sciences

Bing Zhang
Department of Physics and Astronomy, University of Nevada, Las Vegas, Las Vegas, NV 89154,USA

Sarah Burke-Spolaor
Jet Propulsion Laboratory https://orcid.org/0000-0003-4052-7838

Casey Law
Cahill Center for Astronomy and Astrophysics, MC 249-17 California Institute of Technology

Ryan Lynch
NRAO Green Bank https://orcid.org/0000-0001-5229-7430

Liam Connor
California Institute of Technology https://orcid.org/0000-0002-7587-6352

Reshma Anna-Thomas
Department of Physics and Astronomy, West Virginia University; Center for Gravitational Waves and Cosmology, West Virginia University

Lei Zhang
https://orcid.org/0000-0001-8539-4237

Ran Duan

CAS Key Laboratory of FAST, NAOC, Chinese Academy of Sciences

Jumei Yao

National Astronomical Observatories, Chinese Academy of Sciences, Beijing 100101, China
https://orcid.org/0000-0002-4997-045X

Chao-Wei Tsai

National Astronomical Observatories, Chinese Academy of Sciences, Beijing 100101, China

Weiwei Zhu

Chinese Academy of Sciences https://orcid.org/0000-0001-5105-4058

Marilyn Cruces

Max-Planck-Institut fu r Radioastronomie, Auf dem Hu gel 69, D-53121 Bonn, Germany
https://orcid.org/0000-0001-6804-6513

George Hobbs

CSIRO https://orcid.org/0000-0003-1502-100X

C.C. Miao

National Astronomical Observatories, Chinese Academy of Sciences

J.R. Niu

National Astronomical Observatories, Chinese Academy of Sciences

Miroslav Filipovic

Western Sydney University https://orcid.org/0000-0002-4990-9288

Shiqiang Zhu

Zhejiang Lab

Article

Keywords:

Posted Date: May 12th, 2022

DOI: https://doi.org/10.21203/rs.3.rs-1436439/v1

Magnetic Field Reversal around an Active Fast Radio Burst

S. Dai[1,3,15]*; Y. Feng[2]*; Y. P. Yang[4]*; Y. K. Zhang[3,5,2]*; D. Li[3,2,5,10]✉, C. H. Niu[3], P. Wang[3], M. Y. Xue[3], B. Zhang[6,7], S. Burke-Spolaor[8,9,10], C. J. Law[11,12], R. S. Lynch[13], L. Connor[11], R. Anna-Thomas[8,9], L. Zhang[3], R. Duan[3], J. M. Yao[3], C. W. Tsai[3], W. W. Zhu[3], M. Cruces[14], G. Hobbs[15], C. C. Miao[3], J. R. Niu[3], M. D. Filipović[1], S. Q. Zhu[16]

[1]*School of Science, Western Sydney University, Locked Bag 1797, Penrith, NSW 2751, Australia*

[2]*Research Center for Intelligent Computing Platforms, Zhejiang Laboratory, Hangzhou 311100, China*

[3]*National Astronomical Observatories, Chinese Academy of Sciences, Beijing 100101, China*

[4]*South-Western Institute for Astronomy Research, Yunnan University, Kunming 650500, Yunnan, China*

[5]*University of Chinese Academy of Sciences, Beijing 100049, China*

[6]*Nevada Center for Astrophysics, University of Nevada, Las Vegas, NV 89154, USA*

[7]*Department of Physics and Astronomy, University of Nevada, Las Vegas, NV 89154, USA*

[8]*Department of Physics and Astronomy, West Virginia University, P.O. Box 6315, Morgantown, WV 26506, USA*

[9]*Center for Gravitational Waves and Cosmology, West Virginia University, Chestnut Ridge Research Building, Morgantown, WV 26505, USA*

[10]*Canadian Institute for Advanced Research, CIFAR Azrieli Global Scholar, MaRS Centre West*

Email:dili@nao.cas.cn, orcid.org/0000-0003-3010-7661

*These authors contributed equally to this work.

Tower, 661 University Ave. Suite 505, Toronto ON M5G 1M1, Canada

[11]*Cahill Center for Astronomy and Astrophysics, MC 249-17 California Institute of Technology, Pasadena, CA 91125, USA*

[12]*Owens Valley Radio Observatory, California Institute of Technology, 100 Leighton Lane, Big Pine, CA, 93513, USA*

[13]*Green Bank Observatory, PO Box 2, Green Bank, WV, 24401, USA*

[14]*Max-Planck-Institut für Radioastronomie, Auf dem Hügel 69, D-53121 Bonn, Germany*

[15]*CSIRO Space and Astronomy, Australia Telescope National Facility, PO Box 76, Epping, NSW 1710, Australia*

[16]*Zhejiang Lab, Hangzhou, Zhejiang 311121, China*

[17]*NAOC-UKZN Computational Astrophysics Centre, U. of KwaZulu-Natal, Durban 4000, South Africa*

The environment of actively repeating fast radio bursts (FRBs) has been shown to be complex and varying[1]. The recently localized FRB 20190520B[2] is extremely active, has the largest confirmed host dispersion measure, and is only the second FRB source associated with a compact, persistent radio source (PRS). The main tracer of the magneto-ionic environments is the rotation measure (RM), a path-integral of the line-of-sight component of magnetic field strength (B) and electron density, which does not allow a direct probe of the B-field configuration. Here we report direct evidence for a B-field reversal based on the observed sign change and extreme variation of FRB 20190520B's RM, which changed from $\sim 10000\,\mathrm{rad\,m^{-2}}$ to $\sim -16000\,\mathrm{rad\,m^{-2}}$ between June 2021 and January 2022. Such extreme RM reversal has

never been observed before in any FRB nor in any astronomical object. The implied short-term change of the B-field configuration in or around the FRB could be due to the vicinity of massive black holes, or a magnetized companion star in binary systems, or a young supernova remnant along the line of sight.

FRB 20190520B is an extremely active repeating FRB hosted by a dwarf galaxy of high specific star formation rate at a redshift $z = 0.241$[2]. Similar to FRB 20121102A[3], the estimated host galaxy dispersion measure (DM_{host}) is substantially higher than that from the inter-galactic-medium (IGM), with FRB 20190520B being the more extreme case with a $DM_{host} \approx 902^{+88}_{-128}\,pc\,cm^{-3}$, nearly an order of magnitude higher than the average of FRB host galaxies[4]. Among all known FRBs, only FRB 20121102A and FRB 20190520B have confirmed compact, persistent radio source (PRS)[5–7], suggesting a distinctive origin or an earlier evolutionary stage for this type of sources[8].

FRB 20190520B was discovered by the Five-hundred-meter Aperture Spherical radio Telescope (FAST[9]) in 1.2 GHz band, but its RM was first measured[10,11] with the Robert C. Byrd Green Bank Telescope (GBT). We attributed such apparent frequency evolution of polarization to multi-path scattering[10]. We have been monitoring FRB 20190520B with the Parkes radio telescope (Murriyang) using its Ultra-Wideband Low (UWL) receiver since April 2020. Our observations covered frequencies from 704 MHz to 4032 MHz (see Methods for details), which enabled us to search for bursts and their linearly polarised emission over a wide frequency range. A total of eight bursts (Fig. 1) were detected with robust linear polarisation measurements (S/N > 5 in terms

of polarized intensity) during four observing sessions from June 2021 to January 2022. All eight bursts were detected above 2.8 GHz with an emission bandwidth ranging from ~ 500 to 1000 MHz. While some bursts show simple and narrow peaks (< 1 ms), others show multiple components with clear structures in frequency as observed in other repeating FRBs [12,13]. The time of arrival (ToA), peak flux density, burst width, dispersion measure (DM), RM, the central frequency weighted by pulse shape in the frequency domain, and degree of de-biased linear and circular polarization of each pulse are listed in Table 1.

Table 1: **Polarization Properties of the eight bursts.** Column (1): burst index; Col.(2): Modified Julian dates referenced to infinite frequency at the Solar System barycentre; Col.(3): peak flux density; Col.(4): burst width; Col.(5): dispersion measure; Col.(6): frequency of the burst weighted by signal to noise ratio.; Col.(7): RM obtained by RM-synthesis; Col.(8): RM obtained by Stokes QU-fitting; Col.(9): degree of linear polarization; Col.(10): degree of circular polarization.

Burst	MJD	$S_{\rm peak}$ (mJy)	Width (ms)	DM ($\rm cm^{-3}$ pc)	Frequency (MHz)	$\rm RM_{FDF}$ ($\rm rad\ m^{-2}$)	$\rm RM_{QUfit}$ ($\rm rad\ m^{-2}$)	% Linear	% Circular
1	59373.6101602727	979.3	1.2	1202.4 ± 0.2	3402	12956^{+143}_{-137}	12298^{+74}_{-93}	30.0 ± 3.1	−2.6 ± 3.0
2	59373.6119604420	2016.6	2.6	1209.6 ± 0.2	3264	12556^{+58}_{-54}	12523^{+40}_{-42}	19.4 ± 1.1	−1.1 ± 1.0
3	59373.6527697290	752.7	1.9	1211.4 ± 0.5	2813	11756^{+31}_{-42}	11743^{+34}_{-37}	25.5 ± 3.2	3.5 ± 3.1
4	59384.6333777010	1051.6	4.2	1212.4 ± 0.2	3485	8054^{+179}_{-166}	8044^{+19}_{-25}	33.7 ± 4.4	−9.2 ± 4.2
5	59400.4348331362	1853.2	1.5	1205.7 ± 0.2	3163	10135^{+76}_{-102}	9608^{+91}_{-73}	15.0 ± 1.8	3.1 ± 1.8
6	59400.4786563295	2020.5	2.3	1206.4 ± 0.2	3801	9715^{+115}_{-88}	9908^{+96}_{-86}	24.4 ± 2.2	−0.5 ± 2.1
7	59588.8344457013	656.5	0.9	1186.0 ± 0.2	3224	-15518^{+84}_{-164}	-16081^{+18}_{-18}	56.7 ± 12.5	1.7 ± 10.8

8	59588.9067463214	1276.4	0.9	1186.4 ± 0.3	3746	-16358^{+298}_{-108}	-16289^{+17}_{-18}	53.2 ± 14.0	-12.8 ± 11.7

During three GBT observations over roughly the same time span, significant RM variations on months time scale have been seen[11]. The Parkes bursts exhibit more extreme variations and sign-reversal over the course of several months. As shown in Fig. 2, the measured RM increased rapidly from $\sim 3000\,\mathrm{rad\,m^{-2}}$ in March 2021[10] to $\sim 10000\,\mathrm{rad\,m^{-2}}$ in June 2021, and then turned over and reversed to $\sim -16000\,\mathrm{rad\,m^{-2}}$ in the next six months. The reversal of RM with a peak-to-peak variation on the order of $10^4\,\mathrm{rad\,m^{-2}}$ in such a short time-scale, which cannot be explained by density fluctuation alone, and thus requires reversal of the B-field direction, has never been observed in FRBs or any other astronomical phenomenon.

Extreme RM greater than $10^4\,\mathrm{rad\,m^{-2}}$ has only been observed in FRB 20121102A[1,14] and in the vicinity of supermassive black holes[15,16]. FRB 20190520B also exhibits RM variations on day to day and week to week timescales, similar to FRB 20121102A[14]. However, the RM of FRB 20121102A decreased almost monotonously, without any reversal, from $1.46\times10^5\,\mathrm{rad\,m^{-2}}$ to $9.7\times10^4\,\mathrm{rad\,m^{-2}}$ between January 2017 and August 2019, dropping by an average of 15% $\mathrm{year^{-1}}$. No RM reversal has been observed in the vicinities of supermassive black holes either. The reversal and large variations of RM cannot be explained solely by the variation in electron density since the DM only varied by $< 20\,\mathrm{pc\,cm^{-3}}$ during this period of time as shown in the panel A of Fig. 2 (see Methods for details of DM measurements).

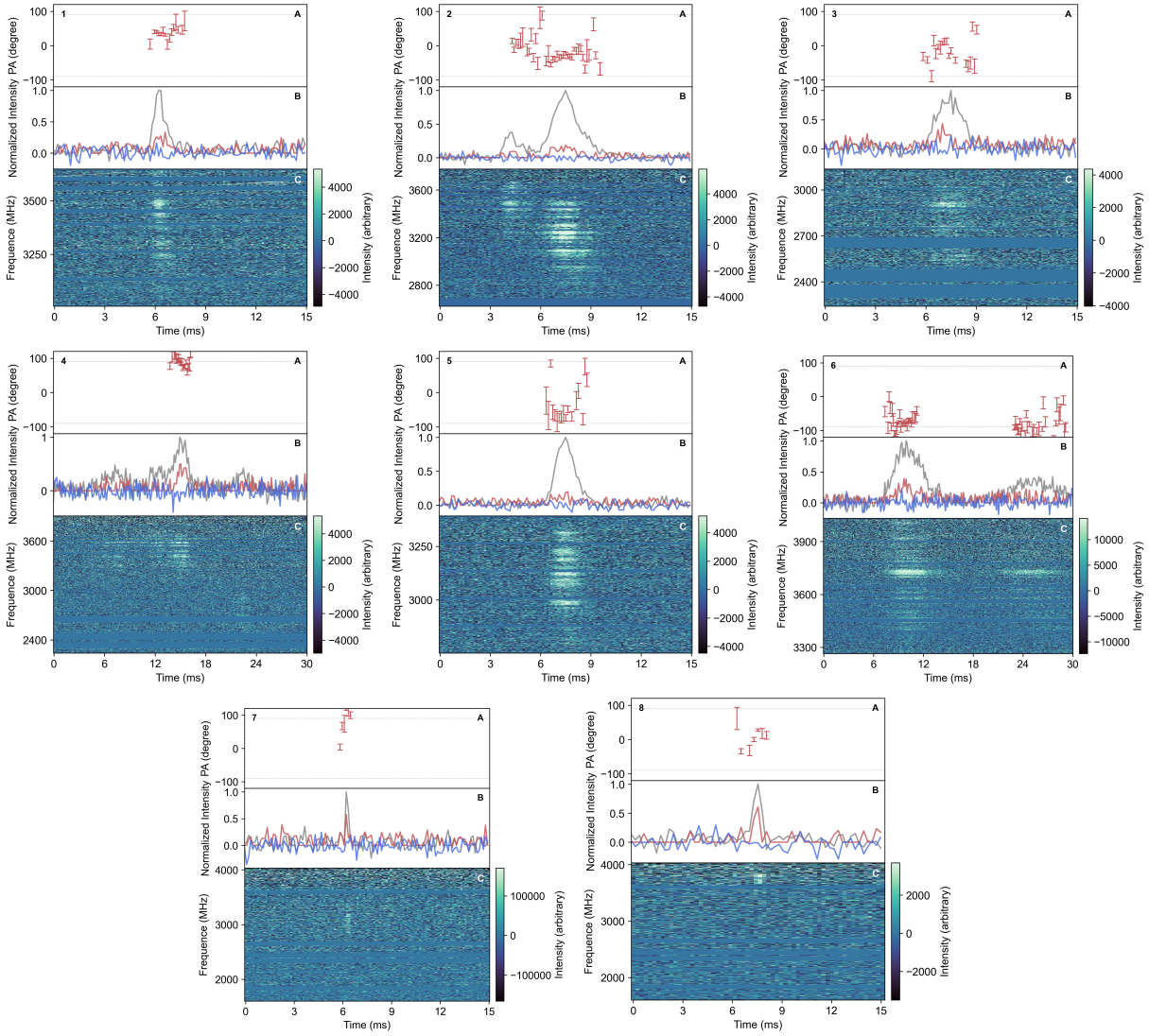

Figure 1: **Polarization profiles and dynamic spectra of the eight bursts from FRB 20190520B.** A, Polarization position angles. B, Polarization pulse profiles; black, red and blue curves denote total intensity, linear polarization and circular polarization, respectively. C, Dynamic spectra.

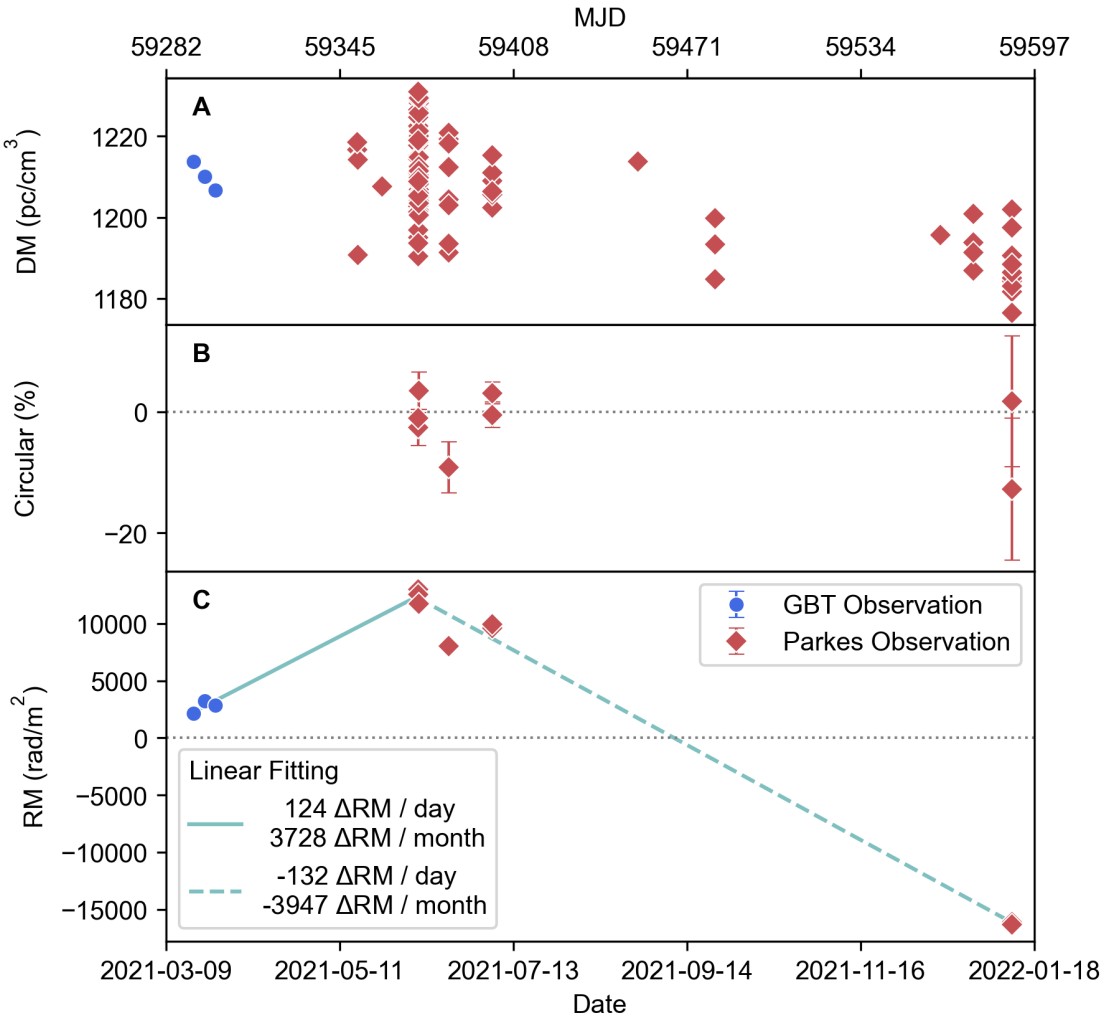

Figure 2: **DMs, circular polarization, and RMs of FRB 20190520B as a function of time.** **A**, DMs of all bursts as a function of time. Blue points denote bursts detected with GBT observations[10]. Red points denote bursts detected with Parkes observations. **B**, Circular polarization of the eight bursts with linear polarisation (S/N > 5 for the linear polarization intensity) as a function of time. **C**, RMs of the eight bursts as a function of time. The solid green line represents linear fitting of RM from MJD 59300 to MJD 59373. The dashed green line represents linear fitting of RM from MJD 59373 to MJD 59588.

Complex magneto-ionic environments have been inferred from observations for some repeaters in previous work[1,8,13]. However, since the magnetic field strength and direction are degenerate, one cannot probe the geometric structure of the magnetic fields directly, even with both RMs and DMs measured, if the RM sign remains unchanged. The observed RM reversal of FRB 20190520B reveals that the RM evolution is mainly due to the change of the geometric configuration of the magnetic field along the line of sight. Meanwhile, extremely large RM values of RM $\sim 10^4$ rad m^{-2} reversing sign during half a year further implies that there must be a strong B field with complex geometric configuration at small scales.

We consider that the relative velocity between the FRB source and the foreground magnetized plasma medium might range from $v \sim (100 - 10^4)$ km s^{-1}. The lower end of 100 km s^{-1} corresponds to the kick velocity of a neutron star [17] and the upper end of 10^4 km s^{-1} the expanding velocity of a young supernova [18]. For the scenarios of the interstellar medium or stellar wind as the foreground, the velocities are also in the above range. Thus, the typical geometric lengthscale of the magnetic field can be estimated as $l \sim v\Delta t \sim (10^{-4} - 10^{-2})$ pc.

For the magneto-ionic cold plasma, the RM is

$$\mathrm{RM} = 0.81 \text{ rad m}^{-2} \int_0^d \frac{B_\parallel(l) n_e(l)}{(1+z(l))^2} dl, \tag{1}$$

where l is the line-of-sight position; $B_\parallel$ is the line-of-sight magnetic field strength in microgausss; n_e is the electron density; z is the redshift of the source; and d is the distance to the source in parsecs. Due to RM $\sim 10^4$ rad m^{-2} and $l \sim (10^{-4} - 10^{-2})$ pc, one has $\xi_{nB} \equiv n_e B_\parallel \sim (10^6 - 10^8)$ cm$^{-3}\mu$G according to Eq.(1). In the interstellar medium, the magnetic field is about a few

μG and the electron density is $\lesssim 10^4$ cm^{-3} (this upper limit corresponds to the observed maximum density of HII regions) [18]. Thus, the resulting $\xi_{nB} \sim (10^6 - 10^8)$ cm$^{-3}\mu$G implies that the RM-generating magneto-ionic medium has to be extremely dense. Furthermore, we parametrize the relation between the magnetic field pressure and gas pressure with $n_e k_B T = \beta B^2/8\pi$, where k_B is the Boltzman constant, and β is a scaling factor with $\beta = 1$ under the energy equipartition. Then one obtains the magnetic field strength as $B \sim (8\pi k_B T \xi_{nB} \beta^{-1})^{1/3} \sim (0.3 - 1.5)\beta^{-1/3}$ mG for a photo-ionized temperature with $T \sim 10^4$ K and $B \gtrsim (1.5 - 7)\beta^{-1/3}$ mG for a shock temperature with $T \gtrsim 10^6$ K depending on the shock evolution [18].

We consider here two feasible astrophysical scenarios (see Methods for details): 1) an FRB source with a magnetic companion, e.g. a massive black hole or a stellar source with extreme magnetized environment. 2) an expanding supernova remnant (SNR) in front of the FRB source. The extremely large RMs with RM $\gtrsim 10^4$ rad m^{-2} have been observed in the vicinities of massive black holes [15,16,19]. If the FRB source is near a massive black hole, the RM variation is accounted for by the change of the parallel field due to the orbital motion around the black hole, and the persistent radio emission may be associated with the black hole itself [20]. On the other hand, the FRB source can also be in a binary system with period of a few years. A magnetized companion star can generate a field reversal along the line of sight. The radio observations of PSR B1259-63 showed that its RM reached an extreme value of a few times 10^3 rad m^{-2} and significantly reversed around periastron [21]. In this case, the observed DM and RM variation would be periodic, which could be tested in future observations. The latter scenario requires a young SNR, but not necessarily the progenitor of the FRB source. The localization of FRB 20190520B constrains

the PRS and FRB source to be within ∼1 kpc^2, and the scattering time scale observed can be well interpreted by a more compact configuration at $\lesssim$100 pc[22]. This is consistent with the FRB propagating in a plasma screen, like an SNR [23]. A young SNR would imply that its DM and the maximum absolute value of the RM will decrease with evolution on longer time scales[24,25].

In summary, the extreme sign-change of the measured RM sheds critical lights into the geometric configuration of the magnetic field around and toward FRB 20190520B. Between the observer and the FRB source, there has to be a dense, highly magnetized (likely ∼mG as opposed to ∼ μG for the general ISM) medium, which also has to be close to the FRB source. Conceivable scenarios include a FRB source in the vicinity of a blackhole or magnetized stellar companion, or an FRB propagating young SNR. Further monitoring can clearly distinguish between these scenarios, in terms of DM variations, periodicity or lack thereof in RM variations, etc.

1. Michilli, D. et al. An extreme magneto-ionic environment associated with the fast radio burst source FRB 121102. *Nature* **553**, 182–185 (2018). 1801.03965.

2. Niu, C. H. et al. A repeating fast radio burst in a dense environment with a compact persistent radio source. arXiv e-prints arXiv:2110.07418 (2021). 2110.07418.

3. Tendulkar, S. P. et al. The Host Galaxy and Redshift of the Repeating Fast Radio Burst FRB 121102. *Astrophys. J. Lett.* **834**, L7 (2017). 1701.01100.

4. Luo, R., Lee, K., Lorimer, D. R. & Zhang, B. On the normalized FRB luminosity function. *Mon. Not. R. Astron. Soc.* **481**, 2320–2337 (2018). 1808.09929.

5. Spitler, L. G. et al. A repeating fast radio burst. *Nature* **531**, 202–205 (2016). 1603.00581.

6. Chatterjee, S. et al. A direct localization of a fast radio burst and its host. *Nature* **541**, 58–61 (2017). 1701.01098.

7. Marcote, B. et al. The Repeating Fast Radio Burst FRB 121102 as Seen on Milliarcsecond Angular Scales. *Astrophys. J. Lett.* **834**, L8 (2017). 1701.01099.

8. Xu, H. et al. A fast radio burst source at a complex magnetised site in a barred galaxy. arXiv e-prints arXiv:2111.11764 (2021). 2111.11764.

9. Li, D. et al. FAST in Space: Considerations for a Multibeam, Multipurpose Survey Using China's 500-m Aperture Spherical Radio Telescope (FAST). IEEE Microwave Magazine **19**, 112–119 (2018). 1802.03709.

10. Feng, Y. et al. Frequency Dependent Polarization of Repeating Fast Radio Bursts – Implications for Their Origin. arXiv e-prints arXiv:2202.09601 (2022). 2202.09601.

11. Anna-Thomas, R. et al. A Highly Variable Magnetized Environment in a Fast Radio Burst Source. arXiv e-prints arXiv:2202.11112 (2022). 2202.11112.

12. Hessels, J. W. T. et al. FRB 121102 Bursts Show Complex Time-Frequency Structure. *Astrophys. J. Lett.* **876**, L23 (2019). 1811.10748.

13. Luo, R. et al. Diverse polarization angle swings from a repeating fast radio burst source. *Nature* **586**, 693–696 (2020). 2011.00171.

14. Hilmarsson, G. H. et al. Rotation Measure Evolution of the Repeating Fast Radio Burst Source FRB 121102. *Astrophys. J. Lett.* **908**, L10 (2021). 2009.12135.

15. Bower, G. C., Wright, M. C. H., Falcke, H. & Backer, D. C. Interferometric Detection of Linear Polarization from Sagittarius A* at 230 GHz. *Astrophys. J.* **588**, 331–337 (2003). astro-ph/0302227.

16. Marrone, D. P., Moran, J. M., Zhao, J.-H. & Rao, R. An Unambiguous Detection of Faraday Rotation in Sagittarius A*. *Astrophys. J. Lett.* **654**, L57–L60 (2007). astro-ph/0611791.

17. Cordes, J. M. & Chernoff, D. F. Neutron Star Population Dynamics. II. Three-dimensional Space Velocities of Young Pulsars. *Astrophys. J.* **505**, 315–338 (1998). astro-ph/9707308.

18. Draine, B. T. Physics of the Interstellar and Intergalactic Medium (Princeton University Press, 2011).

19. Eatough, R. P. et al. A strong magnetic field around the supermassive black hole at the centre of the Galaxy. *Nature* **501**, 391–394 (2013). 1308.3147.

20. Zhang, B. FRB 121102: A Repeatedly Combed Neutron Star by a Nearby Low-luminosity Accreting Supermassive Black Hole. *Astrophys. J. Lett.* **854**, L21 (2018). 1801.05436.

21. Johnston, S. et al. Radio observations of PSR B1259-63 around periastron. *Mon. Not. R. Astron. Soc.* **279**, 1026–1036 (1996).

22. Ocker, S. K. et al. The Large Dispersion and Scattering of FRB 20190520B are Dominated by the Host Galaxy. arXiv e-prints arXiv:2202.13458 (2022). 2202.13458.

23. Yang, Y.-P., Lu, W., Feng, Y., Zhang, B. & Li, D. Temporal Scattering, Depolarization, and Persistent Radio Emission from Magnetized Inhomogeneous Environments Near Repeating Fast Radio Burst Sources. arXiv e-prints arXiv:2202.09602 (2022). 2202.09602.

24. Yang, Y.-P. & Zhang, B. Dispersion Measure Variation of Repeating Fast Radio Burst Sources. *Astrophys. J.* **847**, 22 (2017). 1707.02923.

25. Piro, A. L. & Gaensler, B. M. The Dispersion and Rotation Measure of Supernova Remnants and Magnetized Stellar Winds: Application to Fast Radio Bursts. *Astrophys. J.* **861**, 150 (2018). 1804.01104.

Acknowledgements D.L. and Y.F. are supported by NSFC grant No. 11988101, 11725313, by the National Key R&D Program of China No. 2017YFA0402600, and by Key Research Project of Zhejiang Lab No. 2021PE0AC03. S. D. is the recipient of an Australian Research Council Discovery Early Career Award (DE210101738) funded by the Australian Government. Y.P.Y is supported by NSFC grant No. 12003028. C.J.L acknowledges support from the National Science Foundation under Grant No. 2022546. W.W.Z. is supported by National SKA Program of China No.2020SKA0120200 and the NSFC 12041303, 11873067. P.W. is supported by NSFC grant No. U2031117, the Youth Innovation Promotion Association CAS (id. 2021055), CAS Project for Young Scientists in Basic Reasearch (grant YSBR-006) and the Cultivation Project for FAST Scientific Payoff and Research Achievement of CAMS-CAS. J.M.Y. is supported by NSFC grant No. 11903049, and the Cultivation Project for FAST Scientific Payoff and Research Achievement of CAMS-CAS. L.Z. is supported by ACAMAR Postdoctoral Fellowship and the National Natural Science Foundation of China (Grant No. 12103069). M. Cruces, D. Li and W. Zhu acknowledges the support from the CAS-MPG LEGACY project. The Parkes radio telescope (Murriyang) is part of the

Australia Telescope National Facility, which is funded by the Commonwealth of Australia for operation as a National Facility managed by CSIRO. This material is based in-part upon work supported by the Green Bank Observatory which is a major facility funded by the National Science Foundation operated by Associated Universities, Inc.

Author Contributions S.D. and D.L. launched the observation campaign. S.D. searched the bursts and analysed the burst properties. Y.F. and Y.K.Z. conducted the polarization analysis and visualization. Y.F., D.L., S.D. and Y.P.Y led the discussion on the interpretation of the results and writing of the manuscript. Y.P.Y. and B.Z. contributed to theoretical investigations of the physical implications of the observational results. All authors contributed to the analysis or interpretation of the data and to the final version of the manuscript.

Competing Interests The authors declare that they have no competing financial interests.

Methods

Observations The repeating FRB 20190520B is currently being monitored fortnightly at Parkes using the Ultra-Wideband Low (UWL) receiver as part of project P1101 (PI: S. Dai) since April 2021. The UWL system provides a radio frequency coverage from 704 MHz to 4032 MHz [26]. Data were recorded with 2-bit sampling every 32 μs in each of the 1 MHz wide frequency channels (3328 channels in total). The integration time of each observation is $\sim$ 7200 s. Data were coherently de-dispersed at a DM of 1220.0 pc cm^{-3} with full Stokes information being recorded.

A critical sampling filter bank has been used to produce 26 sub-bands and we removed 5 MHz of the bandpass at each edge of the 26 sub-bands to mitigate aliasing. To measure the differential gains between the signal paths of the two voltage probes, we observed a pulsed noise signal injected into the signal path prior to the first-stage low-noise amplifiers before each observation. The noise signal also provides a reference brightness for each observation. To correct for the absolute gain of the system, we use observations of the radio galaxy 3C 218 (Hydra A); using on- and off-source pointings to measure the apparent brightness of the noise diode as a function of radio frequency. Polarimetric responses of the UWL are derived from observations of PSR J0437−4715 [27] covering a wide range of parallactic angles [28], taken during the commissioning of UWL in 2018 November. The Stokes parameters are in accordance with the astronomical conventions described by (van Straten 2010) [29]. The linear polarization and the position angle (PA) of linear polarization were calculated following Dai et al. (2015)[30]. All data reduction and calibration used the PSRCHIVE [31] software package.

Search procedures The full UWL band was split into multiple subbands for the search of repeating bursts. We used subband bandwidth of 256 MHz, 384 MHz and 512 MHz to optimise our sensitivity to signals with different characteristic bandwidth. The search of repeating bursts was performed using the pulsar searching software package PRESTO [32] on CSIRO's high performance computer facilities. Strong narrow-band and short duration broadband radio-frequency interference (RFI) were identified and marked using the PRESTO routine RFIFIND. We used a 2 s integration time for RFI masking and the default cutoff to reject time-domain and frequency-domain interference was used in our pipeline. We searched a DM range from 1130 to 1280 $\mathrm{cm^{-3}}$ pc with a DM step of 0.2 $\mathrm{cm^{-3}}$ pc. Data were de-dispersed at each of the trial DMs using the PREPDATA routine with RFI removal based on the RFI mask file produced. Single pulse candidates with S/N larger than seven were identified using the SINGLE_PULSE_SEARCH.PY routine for each de-dispersed time series and for boxcar filtering parameters with filter widths ranging from 1 to 300 samples. Burst candidates were manually examined and narrowband and impulsive RFI were manually zapped. To measure the pulse width, we first smoothed the pulse profile with a Savitzky-Golay filter and then measured its width at 10% of the peak. Similarly, the emission bandwidth was measured with the frequency spectrum of each burst.

Dispersion measure The DM of each burst was determined using the DM_PHASE software package*, which maximizes the coherent power in the pulse across the emission bandwidth. From MJD 59300 to 59600, a total of 113 bursts have been detected and we present their DM measurements in Extended Data Tab. 1 and Fig. 2. Detailed studies of this large sample of bursts will be published

*https://github.com/danielemichilli/DM_phase

in future papers.

Extended Data Tab. 1. DM measurements of 113 bursts.

MJD Barycentric	DM (cm^{-3} pc)	MJD Barycentric	DM (cm^{-3} pc)	MJD Barycentric	DM (cm^{-3} pc)
59351.4750170033	1218.5±0.6	59373.6186719499	1211.0±0.3	59384.6294581983	1220.9±0.4
59351.5021431330	1216.7±0.3	59373.6191020361	1204.6±0.3	59384.6306480944	1204.4±0.5
59351.5110725938	1214.5±0.5	59373.6192861348	1217.2±0.2	59384.6333777010	1212.4±0.2
59351.5168879906	1214.2±0.3	59373.6197510004	1202.8±0.3	59384.6465330782	1218.3±0.4
59351.5315930086	1190.7±0.6	59373.6201633430	1209.7±0.3	59384.6500363071	1193.5±0.2
59351.5315930086	1190.7±0.6	59373.6214299823	1205.8±0.4	59384.6646176032	1203.0±0.6
59360.4955229562	1207.6±0.8	59373.6218976407	1212.7±0.2	59400.4225401029	1202.3±0.4
59373.5838717104	1195.0±0.4	59373.6229176433	1214.3±0.4	59400.4294084405	1206.6±0.3
59373.5850684017	1217.5±0.5	59373.6236883589	1190.4±0.4	59400.4337243184	1209.2±0.3
59373.5852747021	1210.2±0.4	59373.6265007697	1217.8±0.6	59400.4348331362	1205.7±0.2
59373.5872505665	1226.5±0.6	59373.6315025370	1215.2±0.3	59400.4408172622	1209.0±0.3
59373.5877579366	1201.3±0.4	59373.6345711752	1220.0±0.3	59400.4736373893	1211.0±0.2
59373.5895305270	1205.3±0.3	59373.6365923377	1228.2±0.4	59400.4736886456	1215.3±0.6
59373.5897958388	1209.6±0.2	59373.6382490036	1229.0±0.5	59400.4786563295	1206.4±0.2
59373.5916443999	1193.6±0.3	59373.6388043999	1201.6±0.6	59453.2009179602	1213.8±0.4
59373.5933619585	1219.0±0.4	59373.6423418338	1214.8±0.3	59481.2794162788	1193.4±0.6
59373.5934607981	1230.9±0.6	59373.6427697294	1200.4±0.4	59481.3165300471	1199.8±0.4
59373.5939531716	1208.8±0.4	59373.6439084083	1201.8±0.5	59481.3307290648	1184.8±0.3
59373.5956878030	1222.5±0.7	59373.6440640982	1212.6±0.4	59562.9907597572	1195.9±0.3

59373.5979591211	1206.0±0.4	59373.6442020997	1204.9±0.2	59562.9912788861	1195.3±0.7
59373.5981310917	1201.7±0.4	59373.6442021552	1204.9±0.2	59562.9999439222	1195.6±0.2
59373.6020685605	1231.1±0.5	59373.6448700063	1218.6±0.5	59574.9781089355	1200.9±0.2
59373.6024451120	1229.6±0.4	59373.6456917126	1206.9±0.4	59574.9815491667	1186.5±0.3
59373.6028841527	1202.5±0.3	59373.6456921157	1204.1±0.4	59574.9831980626	1191.2±0.3
59373.6052884124	1204.0±0.3	59373.6521955553	1210.4±0.6	59574.9945700731	1186.8±0.2
59373.6072687276	1224.4±0.4	59373.6526363122	1208.2±0.3	59575.0300177670	1193.7±0.3
59373.6072690031	1224.4±0.4	59373.6527697290	1211.4±0.5	59575.0354346287	1191.4±0.5
59373.6076421224	1208.0±0.5	59373.6575778495	1205.5±0.4	59588.8344457013	1186.0±0.2
59373.6092077267	1196.6±0.4	59373.6589247000	1221.3±0.4	59588.8524971994	1181.6±0.2
59373.6097061918	1203.9±0.4	59373.6609038940	1203.4±0.4	59588.8583910781	1190.6±0.3
59373.6099189906	1210.9±0.6	59373.6613604095	1200.6±0.4	59588.8665026800	1184.2±0.3
59373.6101602727	1202.4±0.2	59373.6621657088	1225.8±0.3	59588.8742191064	1185.0±0.4
59373.6119604420	1209.6±0.2	59373.6633856556	1205.9±0.4	59588.8947177502	1176.5±0.2
59373.6132582173	1205.6±0.3	59373.6653132433	1229.5±0.4	59588.9035810742	1201.9±0.3
59373.6134620465	1224.7±0.4	59373.6660004684	1209.8±0.3	59588.9040644909	1183.0±0.5
59373.6150713389	1196.8±0.2	59384.5914904468	1191.4±0.6	59588.9067463214	1186.4±0.2
59373.6158102326	1208.9±0.5	59384.6029173974	1203.0±0.4	59588.9117617914	1197.5±0.5
59373.6169866773	1215.5±0.7	59384.6169621390	1219.2±0.4	59588.9244279910	1188.5±0.5

Faraday rotation We searched for an RM detection using the methods of RM-synthesis [33,34] and Stokes QU-fitting [35]. Examples of the results from RM-synthesis are shown in Extended Data Fig. 1 and for Stokes QU-fitting in Extended Data Fig. 2. We find consistent values with both methods (Table 1).

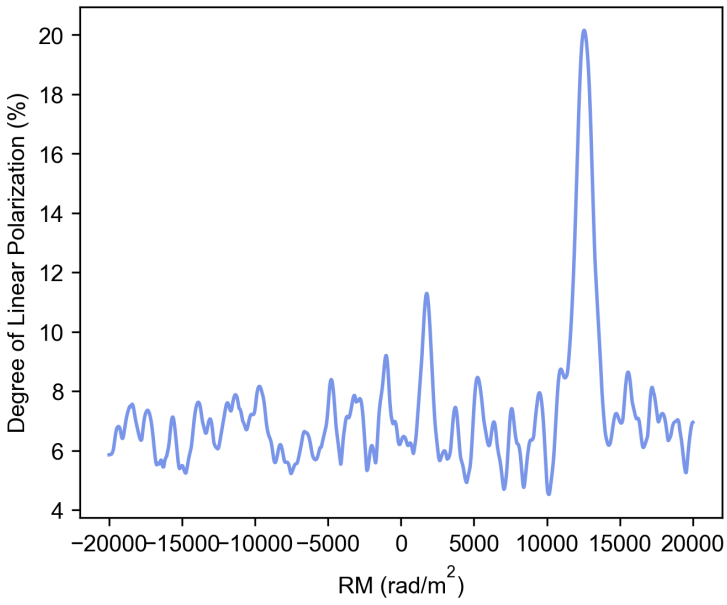

Extended Data Fig. 1. RM search with RM-synthesis. Example result of RM-synthesis. The blues line represents linear polarization fraction of the burst as a function of rotation measure.

We derotated the linear polarization with the measured RM. We then calculated the degrees of linear polarization and circular polarization for each burst. We use the frequency-averaged, de-biased total linear polarization [36]:

$$L_{\text{de-bias}} = \begin{cases} \sigma_I \sqrt{\left(\frac{L_i}{\sigma_I}\right)^2 - 1} & \text{if } \frac{L_i}{\sigma_I} > 1.57 \\ 0 & \text{otherwise,} \end{cases} \tag{2}$$

where σ_I is the Stokes I off-pulse standard deviation and L_i is the measured frequency-averaged linear polarization of time sample i. We defined $I = \Sigma_i I_i$, $L = \Sigma_i L_{\text{de-bias},i}$ and $V = \Sigma_i V_i$, where the summation is over the bursts and V_i is the measured frequency-averaged circular polarization of time sample i. We then defined the degree of linear polarization as L/I and that of circular polarization as V/I. Uncertainties on the linear polarization fraction and circular polarization fraction

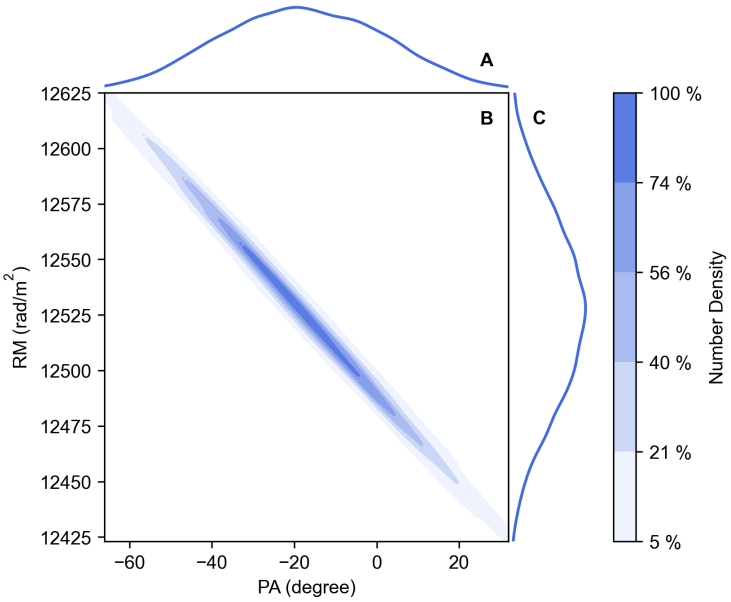

Extended Data Fig. 2. RM search with Stokes QU-fitting. Example result of Stokes QU-fitting for the same bursts shown in Extended Data Fig. 1. **A**, Marginalized posterior of the PA. **B**, Two dimensional posterior probability distributions of the RM and PA. **C**, Marginalized posterior of the RM. The selection of contour levels is displayed in the colour bar.

are calculated as:

$$\sigma_{\rho/I} = \frac{\sqrt{N + N\frac{\rho^2}{I^2}}}{I}\sigma_I, \tag{3}$$

where N is the number of time samples of the burst, and $\rho = L, V$ for linear and circular polarization fraction, respectively. The degrees of linear polarization and circular polarization are listed in Table 1.

Possible astrophysical scenarios In this section, we discuss two possible astrophysical scenarios producing the RM reversal: 1) the RM reversal is contributed by an expanding supernova remnant (SNR), as shown in panel (a) of Figure 3; 2) the RM reversal is due to the change of relative position between an FRB source and its companion, as shown in panel (b) of Figure 3.

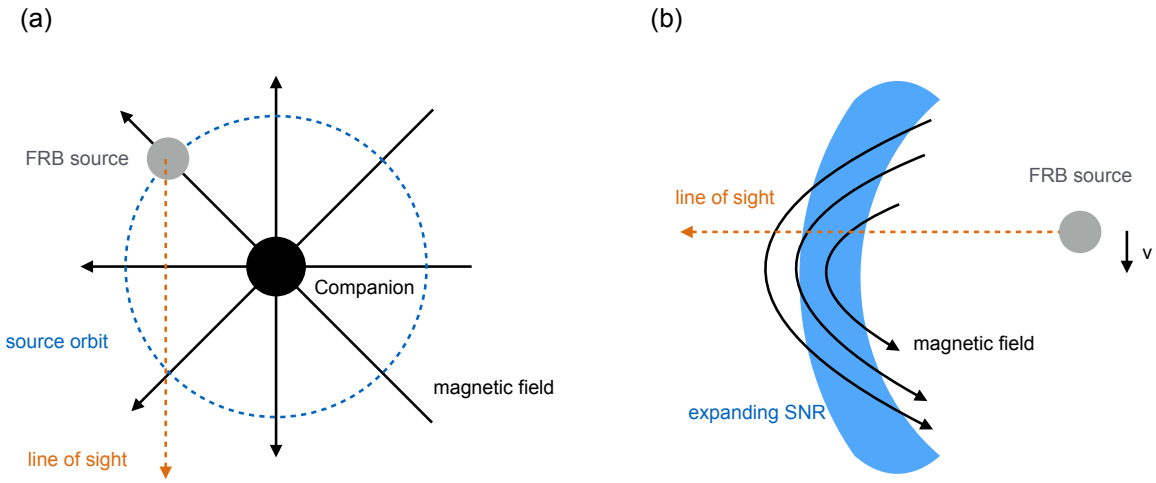

Extended Data Fig. 3. Two possible astrophysical scenarios. Panel (a) the FRB source is in the vicinity of its companion with large-scale magnetic field. Panel (b) an SNR as the foreground of the FRB source.

First, we consider that FRB 20190520B is close to a companion surrounded by magnetized medium, e.g., a massive black hole or a companion star, as shown in panel (a) of Figure 3. In this case, the RM evolution of FRB 20190520B would have a period of a few years, considering that the magnetic field of the companion is large-scale and the observed RM evolution (i.e., RM reversal) is significant during half a year. A long-term monitoring of FRB 20190520B with RM measurements is encouraged to test this scenario. The extreme large RMs with RM $\gtrsim 10^4$ rad m^{-2} have been observed in the vicinities of massive black holes [15,16,19], and the RM variation is accounted for by the change of parallel magnetic field due to the orbital motion of the FRB source around the black hole [20]. The orbital period of the FRB source moving around a massive black hole is $P_{\rm orb} = 2.9\ {\rm yr}(r/10^{-3}\ {\rm pc})^{3/2}(M_{\rm BH}/10^6 M_\odot)^{-1/2}$, where r is the separation between the FRB source and the massive black hole, and $M_{\rm BH}$ is the black hole mass. The timescale of RM reversal is less than the predicted period. On the other hand, the FRB source could be in a binary system with an orbital period of $P_{\rm orb} = 5.4\ {\rm yr}(a/10^{14}\ {\rm cm})^{3/-2}(M_{\rm tot}/10 M_\odot)^{-1/2}$, where a is the semi-major axis, and $M_{\rm tot}$ is the total mass of the binary system. For example, radio observations of PSR B1259−63 showed that its RM reached an extreme value of a few times 10^3rad m^{-2} and significantly reversed around periastron. In this case, the observed DM and RM would exhibit periodic evolution, which could be tested in future observations.

Next, we consider that the RM originates from an expanding SNR along the line of sight of the FRB source. It is noteworthy that some active repeating FRBs (including FRB 20190520B) exhibit conspicuous frequency-dependent linear polarization fraction that can be well described by RM scatter[10], and the relation between RM scatter and temporal scattering for various repeaters

suggests that both of them are due to multi-path progagation through a magnetized inhomogeneous plasma screen [23]. Due to $\sigma_{\rm RM} \ll |{\rm RM}|$, the RM reversal must be mainly caused by the large-scale magnetic field, otherwise, the random small-scale magnetic field would cause $\sigma_{\rm RM} \sim {\rm RM}$, which is inconsistent with the observation of FRB 20190520B.

We take the SNR expanding velocity as $V \sim 10^4$ km s^{-1} and the radius as $R \sim Vt$ with age t, as shown in the panel (b) of Figure 3. Since the dynamic evolution timescale of the SNR, $\tau_{\rm SNR} \sim R/V \sim 10\ {\rm yr}(R/0.1\ {\rm pc})(V/10^4\ {\rm km\ s^{-1}})^{-1}$, is much larger than the observed timescale of the RM reversal $\Delta t \sim 0.5$ yr (unless the SNR is very young with age $\lesssim 1$ yr), the observed RM reversal is dominated by the relative position change of the FRB source and the SNR in the projected plane, as shown in panel (b) of Figure 3. Observations of radio polarization of Galactic SNRs shows that the coherent length of their large-scale magnetic fields is about $\eta \sim (1-10)\%$ of the SNR radius [37,38]. Thus, the typical timescale of the evolution of the projected magnetic field is $\tau_B \sim \eta R/V \sim \eta\tau_{\rm SNR}$. For the RM reversal with timescale of $\tau_B \sim \Delta t \sim 0.5$ yr, the SNR has an age of $\tau_{\rm SNR} \sim \tau_B/\eta \sim 50(\eta/0.01)^{-1}$ yr and a radius of $R \sim V\tau_{\rm SNR} \sim 0.5\ {\rm pc}(\eta/0.01)^{-1}(V/10^4\ {\rm km\ s^{-1}})$, which means that there is a young SNR in free-expansion phase along the line of sight of FRB 20190520B. Meanwhile, the extreme large RM and host DM of FRB 20190520B is also consistent with a young SNR along the line of sight [24,25]. The reasons are as follows: for an SNR with ejecta mass M and radius R during the free-expansion phase, the electron density is $n_e \sim 3M/(4\pi m_p R^3) \sim 10^4\ {\rm cm^{-3}}(M/M_\odot)(R/0.1\ {\rm pc})^{-3}$, and the DM contributed by the SNR is ${\rm DM} \sim n_e R \sim 1000\ {\rm pc\ cm^{-3}}(M/M_\odot)(R/0.1\ {\rm pc})^{-2}$. Since the coherent length of the magnetic field is $l_B \sim \eta R \sim 10^{-3}\ {\rm pc}(\eta/0.01)(R/0.1\ {\rm pc})$ and the observed RM is ${\rm RM} \sim 10^4\ {\rm rad\ m^{-2}}$,

the magnetic field strength might be estimated by $B \sim 1.2\ \mathrm{mG}(\eta/0.01)^{-1}(M/M_{\odot})^{-1}(R/0.1\ \mathrm{pc})^{2}$.

Furthermore, if the young SNR is indeed along the line of sight of the FRB source, there are two possibilities: 1) the SNR is physically associated with the FRB source; 2) the SNR is close to the FRB source, but they do not share the same progenitor. For the former case, the FRB source and the SNR have the same age. The projected distance between the FRB source to the SNR center is $r_{s,\perp} \sim v_{s,\perp}t$, where $v_{s,\perp}$ is the kick velocity of the FRB source perpendicular to the line of sight. Due to $r_{s,\perp}/R \sim v_{s,\perp}/V \sim$ constant, the relative projected position of the FRB source can not significantly change during the observation time. Thus, the RM reversal might not be significant unless the SNR shock is decelerated by the nearby inhomogeneous ambient medium. In the latter case, since the FRB source and the SNR are independent, a large relative motion in the projected plane between them is allowable, leading to the observed RM reversal. In this case, the FRB source could be the companion of the progenitor of the supernova, or they are in the same region of its host galaxy.

Data availability The bursts data are openly available in Science Data Bank at `https://doi.org/10.11922/sciencedb.o00069.00007`.

Code availability Computational programs for the polarization analysis reported here are available at `https://github.com/SukiYume/RMS`. Other standard data reduction packages are available at their respective websites:

PRESTO - `https://github.com/scottransom/presto`;

DSPSR - `http://dspsr.sourceforge.net`;

PSRCHIVE - http://psrchive.sourceforge.net;

DM_PHASE - https://github.com/danielemichilli/DM_phase.

Reference

26. Hobbs, G. et al. An ultra-wide bandwidth (704 to 4 032 MHz) receiver for the Parkes radio telescope. *Publ. Astron. Soc. Aust.* **37**, e012 (2020). 1911.00656.

27. Johnston, S. et al. Discovery of a very bright, nearby binary millisecond pulsar. *Nature* **361**, 613–615 (1993).

28. van Straten, W. Radio Astronomical Polarimetry and Point-Source Calibration. *Astrophys. J. Suppl.* **152**, 129–135 (2004). astro-ph/0401536.

29. van Straten, W., Manchester, R. N., Johnston, S. & Reynolds, J. E. PSRCHIVE and PSRFITS: Definition of the Stokes Parameters and Instrumental Basis Conventions. *Publ. Astron. Soc. Aust.* **27**, 104–119 (2010). 0912.1662.

30. Dai, S. et al. A study of multifrequency polarization pulse profiles of millisecond pulsars. *Mon. Not. R. Astron. Soc.* **449**, 3223–3262 (2015). 1503.01841.

31. Hotan, A. W., van Straten, W. & Manchester, R. N. PSRCHIVE and PSRFITS: An Open Approach to Radio Pulsar Data Storage and Analysis. *Publ. Astron. Soc. Aust.* **21**, 302–309 (2004). astro-ph/0404549.

32. Ransom, S. M. New search techniques for binary pulsars. Ph.D. thesis, Harvard University (2001).

33. Burn, B. J. On the depolarization of discrete radio sources by Faraday dispersion. *Mon. Not. R. Astron. Soc.* **133**, 67 (1966).

34. Brentjens, M. A. & de Bruyn, A. G. Faraday rotation measure synthesis. *Astron. & Astrophys.* **441**, 1217–1228 (2005). astro-ph/0507349.

35. O'Sullivan, S. P. et al. Complex Faraday depth structure of active galactic nuclei as revealed by broad-band radio polarimetry. *Mon. Not. R. Astron. Soc.* **421**, 3300–3315 (2012). 1201.3161.

36. Everett, J. E. & Weisberg, J. M. Emission Beam Geometry of Selected Pulsars Derived from Average Pulse Polarization Data. *Astrophys. J.* **553**, 341–357 (2001). astro-ph/0009266.

37. Dickel, J. R. & Milne, D. K. Magnetic fields in supernova remnants. Australian Journal of Physics **29**, 435–460 (1976).

38. Milne, D. K. An atlas of supernova remnant magnetic fields. Australian Journal of Physics **40**, 771–787 (1987).